2015

New insight into the helium-induced damage in MAX phase Ti_3AlC_2 by first-principles studies

Yiguo Xu
Division of Functional Materials and Nanodevices, Ningbo Institute of Materials Technology and Engineering, Chinese Academy of Sciences, Ningbo, Zhejiang

Xiaojing Bai
Division of Functional Materials and Nanodevices, Ningbo Institute of Materials Technology and Engineering, Chinese Academy of Sciences, Ningbo, Zhejiang

Xianhu Zha
Division of Functional Materials and Nanodevices, Ningbo Institute of Materials Technology and Engineering, Chinese Academy of Sciences, Ningbo, Zhejiang

Qing Huang
Division of Functional Materials and Nanodevices, Ningbo Institute of Materials Technology and Engineering, Chinese Academy of Sciences, Ningbo, Zhejiang, huangqing@nimte.ac.cn

Jian He
Laboratory of Biotechnology, Dalian Institute of Chemical Physics, Chinese Academy of Sciences, Dalian, Liaoning

See next page for additional authors

New insight into the helium-induced damage in MAX phase Ti_3AlC_2 by first-principles studies

Yiguo Xu,[1] Xiaojing Bai,[1] Xianhu Zha,[1] Qing Huang,[1,a)] Jian He,[2] Kan Luo,[1] Yuhong Zhou,[1] Timothy C. Germann,[3] Joseph S. Francisco,[4] and Shiyu Du[1,b)]
[1]*Division of Functional Materials and Nanodevices, Ningbo Institute of Materials Technology and Engineering, Chinese Academy of Sciences, Ningbo, Zhejiang 315201, China*
[2]*Laboratory of Biotechnology, Dalian Institute of Chemical Physics, Chinese Academy of Sciences, Dalian, Liaoning 116023, China*
[3]*Theoretical Division, Los Alamos National Laboratory, Los Alamos, New Mexico 87545, USA*
[4]*College of Art and Sciences, University of Nebraska-Lincoln, Lincoln, Nebraska 68588-0312, USA*

(Received 29 May 2015; accepted 2 September 2015; published online 18 September 2015)

In the present work, the behavior of He in the MAX phase Ti_3AlC_2 material is investigated using first-principle methods. It is found that, according to the predicted formation energies, a single He atom favors residing near the Al plane in Ti_3AlC_2. The results also show that Al vacancies are better able to trap He atoms than either Ti or C vacancies. The formation energies for the secondary vacancy defects near an Al vacancy or a C vacancy are strongly influenced by He impurity content. According to the present results, the existence of trapped He atoms in primary Al vacancy can promote secondary vacancy formation and the He bubble trapped by Al vacancies has a higher tendency to grow in the Al plane of Ti_3AlC_2. The diffusion of He in Ti_3AlC_2 is also investigated. The energy barriers are approximately 2.980 eV and 0.294 eV along the *c*-axis and in the *ab* plane, respectively, which means that He atoms exhibit faster migration parallel to the Al plane. Hence, the formation of platelet-like bubbles nucleated from the Al vacancies is favored both energetically and kinetically. Our calculations also show that the conventional spherical bubbles may be originated from He atoms trapped by C vacancies. Taken together, these results are able to explain the observed formation of bubbles in various shapes in recent experiments. This study is expected to provide new insight into the behaviors of MAX phases under irradiation from electronic structure level in order to improve the design of MAX phase based materials. © *2015 AIP Publishing LLC.* [http://dx.doi.org/10.1063/1.4931398]

I. INTRODUCTION

Ti_3AlC_2 is a typical member of the $M_{n+1}AX_n$ phase materials family, where n = 1, 2, or 3, M is an early transition metal, A is an A-group element, and X is either carbon or nitrogen.[1] Ti_3AlC_2 exhibits a unique combination of metallic and ceramic properties, such as high-temperature stability, good ductility, excellent thermal shock resistance, and intrinsic damage tolerance.[2–5] These unique properties make Ti_3AlC_2 an ideal material for applications under extreme conditions, e.g., in proposed future gas-cooled fast nuclear reactors (GFR) and fusion reactors. Under such conditions, a number of vacancy defects and helium impurities may be continuously produced in structural materials. Helium atoms are insoluble and exhibit low kinetic barriers in materials such as metals; hence, they have a strong tendency to diffuse, aggregate, form bubbles, and finally degrade the mechanical strength of materials.[6] Several studies on He-induced effects of radiation on Ti_3AlC_2 have been conducted in recent years. Patel *et al.* reported the impact of high-fluence (2×10^{17} ions cm^{-2}; 14 at. %) He on Ti_3AlC_2 samples at 500 °C.[7] They found that He implantation disorders the Al layers in polycrystalline Ti_3AlC_2. Wang *et al.*[8] reported radiation damage of 4-52 dpa to Ti_3AlC_2 caused by 50 keV He ions at room temperature. Ti_3AlC_2 showed serious structural disorder but no obvious amorphization. Formation of string-like He bubbles totally different from the spherical bubbles for metals is also observed.[9,10] Song *et al.*[11] found that no amorphization occurs in Ti_3AlC_2 at room temperature, 300 °C or 500 °C under irradiation of 500 keV He ions with doses ranging from 5×10^{16} to 1×10^{18} ions cm^{-2}. Also noteworthy is the observation that He bubbles exhibit spherical, string, and platelet shapes. On the theoretical side, most computational studies have focused on the chemical bonding of defect-free Ti_3AlC_2.[12,13] Few studies have been conducted on the effect of He clusters on the structural stability of Ti_3AlC_2.[14,15] The behavior of He atoms on Ti_3AlC_2 with vacancies is not yet fully understood. Therefore, it is necessary to investigate He behavior in Ti_3AlC_2 to gain a deeper insight into the mechanism of He bubble growth observed in recent experiments.[9–11]

In the present work, we examine the behavior of He atoms on Ti_3AlC_2 using first-principle calculations. The stability, vacancy trapping, and diffusion barriers of He on Ti_3AlC_2 are discussed. Some phenomena observed in recent experiments are explained based on the obtained computational results. The theoretical predictions from this work are expected to be valuable not only for understanding the physical nature of He

a)huangqing@nimte.ac.cn
b)dushiyu@nimte.ac.cn

induced radiation damage in Ti_3AlC_2 but also for improving design and function of Ti_3AlC_2-based materials for industrial applications.

II. METHOD

First-principle electronic structure calculations are performed using density functional theory (DFT) and the pseudopotential plane-wave method implemented in the VASP codes.[16,17] A gradient-corrected form of the exchange correlation functional generalized gradient approximation (GGA-PBE)[18] is employed, and $3 \times 3 \times 1$ supercells composed of 108 atoms are adopted to model defect configurations. The calculations are carried out using the plane-wave cut-off energy of 500 eV. The $5 \times 5 \times 2$ k-point mesh is generated using the Monkhorst-Pack scheme.[19] The energy minimization is converged when atomic forces are less than 0.01 eV/Å. The supercell volume and the atomic positions are fully relaxed in all of the calculations to determine the minimum energy structure. The climbing image nudged elastic-band (CI-NEB) method[20] is used to obtain diffusion pathways and the corresponding energy barriers. Seven intermediate structures (images) between the initial and final configurations are constructed by linear interpolation. All images are optimized along the reaction path simultaneously until the forces acting on the atoms in each image are smaller than 0.05 eV/Å.

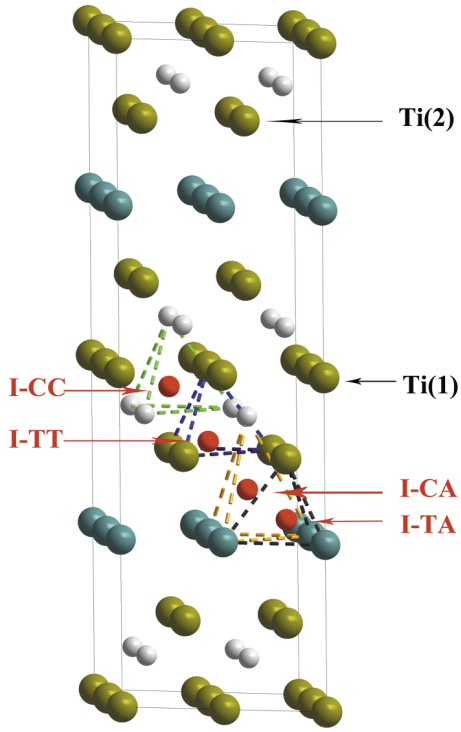

FIG. 1. Crystal structure of Ti_3AlC_2. Interstitial configurations of I-TA, I-CA, I-TT, and I-CC are also depicted by the frames of dashed lines. Red, dark yellow, dark gray, and dark cyan circles present He, Ti, C, and Al atoms, respectively.

III. RESULTS AND DISCUSSION

Ti_3AlC_2 has a hexagonal crystal structure with the P63/*mmc* space group,[21] where Ti occupies the $2a$ and $4f$ Wyckoff position, Al is at the $2b$ Wyckoff position, and C is at the $4f$ Wyckoff position, as shown in Fig. 1. To distinguish the Ti atoms in two different coordination environments, we denote Ti atoms located at $2a$ sites as Ti(1) and Ti atoms at the $4f$ sites as Ti(2). For the fully relaxed Ti_3AlC_2 structure, we obtain the lattice constants of $a = 3.082$ Å and $c = 18.652$ Å, in good agreement with the findings of the previous studies.[12,14] To determine the most stable site for a single He atom in perfect or defective Ti_3AlC_2, we calculate the solution energy for a He atom at different sites. The solution energy for a He atom in Ti_3AlC_2 with and without a vacancy is defined as[22,23]

$$E_i^s(\mathrm{He}) = E_i(ref + \mathrm{He}) - E(ref) - E_{\mathrm{He}} \quad (1)$$

and

$$E_i^s(\mathrm{He}) = E_i(ref + \mathrm{He}, V) - E(ref + V) - E_{\mathrm{He}}, \quad (2)$$

where $E_i(ref + \mathrm{He})$ is the energy of Ti_3AlC_2 with a single He atom at the site i; $E(ref)$ is the energy of a perfect Ti_3AlC_2 crystal; E_{He} is the energy of an isolated He atom; $E_i(ref + \mathrm{He}, V)$ is the energy of Ti_3AlC_2 with a single He atom and a single vacancy at site i; and $E(ref + V)$ is the energy of Ti_3AlC_2 with a single vacancy. Four interstitial positions can accommodate He atoms in Ti_3AlC_2 (Fig. 1): a tetrahedral interstitial site (I-TA) surrounded by one Ti(2) and three Al atoms, a tetrahedral interstitial site (I-CA) surrounded by one Ti(1) and three Al atoms, a tetrahedral interstitial site (I-TT) surrounded by one Ti(1) and three Ti(2) atoms, and a tetrahedral interstitial site (I-CC) surrounded by four C atoms. The calculated solution energies are 2.393 eV, 2.691 eV, 3.154 eV, and 4.880 eV for I-TA, I-CA, I-TT, and I-CC, respectively, indicating that I-TA is the most stable position for a single He interstitial atom in an otherwise perfect Ti_3AlC_2 and that He atom is located near the Al plane in Ti_3AlC_2. These results are in agreement with experimental results, which show that He implantation disordered the Al layers.[7]

As a structural material for nuclear energy applications, Ti_3AlC_2 is inevitably subject to high temperatures and particle fluxes that produce large numbers of vacancies. First-principle calculations have suggested that Al and C vacancies are more readily formed in Ti_3AlC_2.[24,25] For this reason, we consider Al and C vacancies in Ti_3AlC_2 to compare their ability to trap He atoms. The solution energies predicted by our calculations for He at the Al and C vacancy sites are 0.944 eV and 2.035 eV, respectively. These values are both much lower than that of a He atom in perfect Ti_3AlC_2, indicating that He atoms favor being trapped by vacancies. This can be explained by the larger volume available for helium accommodation at the vacancy sites compared to the interstitial sites. This result is in good agreement with the previous theoretical predictions and experimental measurements.[6,22] Additionally, it is important to note that the solution energy of He in an Al vacancy is lower than that of a C vacancy, which implies that the Al vacancy exhibits stronger trapping for He than the C vacancy.

To determine the number of He atoms that a vacancy can accommodate, we also calculate the trapping energy of additional He atoms migrating to the vacancy, which is defined as[22,23]

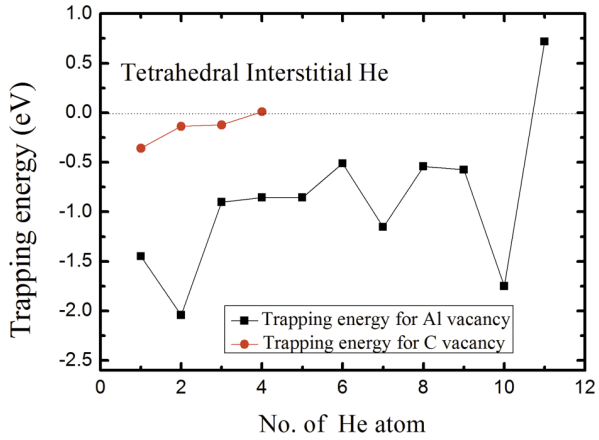

FIG. 2. Trapping energy for He atom as a function of the number of He atoms trapped by a single Al vacancy and a single C vacancy in Ti_3AlC_2.

$$E_{trap} = E(ref + n\mathrm{He}, V) - E(ref + (n-1)\mathrm{He}, V) - E_{I-TA}(ref + \mathrm{He}) + E(ref), \quad (3)$$

where $E(ref + n\mathrm{He}, V)$ is the energy of Ti_3AlC_2 with n He atoms and a single vacancy and $E_{I-TA}(ref + \mathrm{He})$ is the energy of Ti_3AlC_2 with one He atom in the interstitial site I-TA. The I-TA site is adopted here because it has been determined to be the most stable interstitial site for one He atom. A negative value for the trapping energy represents the energy gained by the system when a He atom is trapped at a single vacancy site relative to the case when the He atom is located at an interstitial site. The trapping energy as a function of the number of He atoms in an Al or a C vacancy is illustrated in Fig. 2 and shows that He atom trapping by an Al vacancy is exothermic until the number of He atoms reaches 11, suggesting that up to 10 He atoms can be trapped by an Al vacancy. On the other hand, it is energetically favorable for a C vacancy to trap up to three He atoms, but when the fourth He atom is added, the trapping energy becomes positive (0.012 eV), showing the trapping is energetically unfavorable. Therefore, only three He atoms can be trapped by a C vacancy. This further demonstrates that the Al vacancies exhibit a stronger helium trapping ability than the C vacancies, as indicated both by the calculated energy gain per He atom and by the number of He atoms that can be accommodated. The tendency for He atoms to aggregate and reside near the Al plane, forming He bubbles, explains the observed disorder of Ti_3AlC_2 in the Al layers after He irradiation.[7]

In order to gain deeper understanding on the interaction mechanism, the trapping of He atoms in MAX phases, the influence of He atoms trapped at a Al or C vacancy on the crystalline structure of Ti_3AlC_2 is investigated. Table I lists lattice parameters and volumes of a Ti_3AlC_2 unit cell varying with different number of trapped He atoms. When an Al vacancy is formed, the lattice parameter changes along a-axis direction and c-axis direction are 0.1416% and −0.2955%, respectively, and the volume change is −0.0129%, exhibiting a weak anisotropic contraction. When one He atom is added to an Al vacancy, the volume increases by 0.2731%, showing an expansion. When there exist more than one He atoms, the volume continues to expand anisotropically until ten He atoms are trapped and the maximum volume change of 3.2284% is reached. Similarly, when a C vacancy is introduced, the lattice parameters changes along a-axis direction and along c-axis direction are −0.053% and −0.0240%, and the volume decreases by 0.1307%. Therefore, a C vacancy can cause more volume change in the structure of Ti_3AlC_2. When He atoms are implanted into a C vacancy, the volume of the crystal expands by 0.1614% (with one He atom trapped) to 0.8292% (with three He atoms trapped). Thus, the volume changes for the structure with a C vacancy are larger than those with an Al vacancy when two or more He atoms are trapped. It means that He atoms trapped at C vacancy may cause greater strain on the structure of Ti_3AlC_2, leading to more energy change of the system. Therefore, He atom is energetically unfavorable to be trapped by C vacancy. It provides an explanation from the structural perspective that Al vacancy exhibits a stronger He trapping ability than the C vacancy. It can also be understood from the electronic structures of the He–Ti_3AlC_2 system. The C

TABLE I. Summary of lattice parameters and volume varying of with increasing number of trapped He atoms in a Al or C vacancy.

Configuration	a (Å)	c (Å)	V (Å^3)	Δa/a (%)	Δc/c (%)	ΔV/V (%)
Ti_3AlC_2	3.0820	18.6524	1380.9070	0	0	0
V_{Al}	3.0863	18.5973	1380.7294	0.1416	−0.2955	−0.012 9
$V_{Al}1 + 1He$	3.0887	18.6222	1384.6793	0.2176	−0.1621	0.273 1
$V_{Al}1 + 2He$	3.0890	18.6205	1384.8727	0.2293	−0.1715	0.287 11
$V_{Al}1 + 3He$	3.0926	18.6469	1389.8644	0.3449	−0.0295	0.648 7
$V_{Al}1 + 4He$	3.0939	18.6778	1394.0146	0.3886	0.1362	0.949 2
$V_{Al}1 + 5He$	3.0978	18.7098	1399.4139	0.5144	0.3073	1.340 2
$V_{Al}1 + 6He$	3.1007	18.7268	1404.3942	0.6072	0.3985	1.700 9
$V_{Al}1 + 7He$	3.1060	18.7865	1410.9182	0.7801	0.7188	2.173 3
$V_{Al}1 + 8He$	3.1087	18.8386	1417.1187	0.8664	0.9983	2.622 3
$V_{Al}1 + 9He$	3.1126	18.8264	1422.8900	0.9938	0.9329	3.040 2
$V_{Al}1 + 10He$	3.1122	18.8721	1425.4876	0.9805	1.1781	3.228 4
V_C	3.0803	18.6479	1379.1016	−0.053	−0.0240	−0.130 7
$V_C1 + 1He$	3.0838	18.6605	1383.1356	0.0591	0.0431	0.161 4
$V_C1 + 2He$	3.0879	18.6635	1387.0824	0.1935	0.0595	0.447 2
$V_C1 + 3He$	3.0949	18.6697	1392.3570	0.4199	0.0923	0.829 2

atom and Ti atom form a strong covalent C–Ti bond. Therefore, when a C vacancy is present, the electron density inside the vacancy is localized whether He atoms are trapped or not. As to the case of Al, it can form metallic bonds with adjacent atoms. So it is reasonable to expect that the electrons are more delocalized when an Al vacancy is formed. This means that the electrons may be redistributed to adjacent atoms in Ti_3AlC_2, when multiple He atoms are trapped in an Al vacancy. Since He atom has an inert electron configuration, it tends to reside to the place with lower electron density in order to lower the energy of the system. As a result, Al vacancy has a better ability to trap He atoms.

In metals, He clusters homogeneously grow by self-trapping in vacancies of the lattice in a three dimensional space and then only form spherical He bubbles.[9,10] This is drastically different from the experimental observations of Ti_3AlC_2 after He irradiation, where platelet or string-like He bubbles are also formed.[8,11] To reveal how He bubbles evolve in Ti_3AlC_2 and understand the influence of He bubbles on its structural evolution, additional calculations of the Ti_3AlC_2 structures with both He atoms and vacancies are carried out in this work. As mentioned before, Al and C vacancies can be readily formed in Ti_3AlC_2. Therefore, we first introduce either an Al vacancy or a C vacancy in Ti_3AlC_2. Next, the secondary vacancy defect formation energy is calculated for the Al, Ti, and C atoms nearest to the primary Al or C vacancy. The secondary defect formation energy is defined as

$$E_f(V_A) = E(V_{A+B}) - E(V_B) + \mu_A, \tag{4}$$

where $E(V_{A+B})$ is the energy of the system with a first vacancy of species B (B = Al or C) and a secondary vacancy of species A. $E(V_B)$ is the energy of the system with the first vacancy of species B and μ_A is the chemical potential of species A. The defect formation energies are critically dependent on the chemical potential.[26–28] In our study, hexagonal close-packed bulk Ti, face-centered cubic bulk Al, and graphite C are adopted as the reference elemental Ti, Al, and C solids, respectively. The secondary defect formation energies for Ti, Al, and C vacancies as a function of the number of He atoms at the primary Al vacancy are shown in Fig. 3(a). As seen from the figure, the secondary defect formation energies of an Al vacancy near the primary Al vacancy are significantly influenced by the He impurity content. When no He atom is placed at the Al vacancy, the secondary defect formation energy for Al is approximately 2.504 eV. With increasing number of He atoms, the defect formation energy rapidly decreases. When six He atoms are located in an Al vacancy, the subsequent defect formation energy becomes negative (−0.532 eV), reflecting the fact that He-filled primary Al vacancy in Ti_3AlC_2 can promote secondary vacancy formation. For Ti vacancy formation, the secondary defect formation energy exhibits a similar trend. The secondary defect formation energies decrease (but remain positive) with an increasing number of He atoms, from 4.70 eV without any He atoms to 2.21 eV with 10 He atoms, which is the maximum number of He atoms accommodated by an Al vacancy. This means that secondary Ti vacancies will not form spontaneously despite the strong effect of He atoms. By contrast, no obvious dependence of the secondary C vacancy defect formation energies on the number of dissolved He atoms is observed, with the formation energies fluctuating around 2.5 eV. This strongly suggests that the introduction of He atoms does not have a strong impact on the secondary defect formation of C atom near an Al vacancy. This difference can be understood as follows. The Ti atom layer is located next to the Al atom layer, and the C atom layer is farther away from the Al atom layer. Therefore, the effect of a He cluster in a primary Al vacancy on the secondary vacancy defect formation energy will follow the trend of Al > Ti > C. Given the low secondary defect formation energy for Al atoms near the primary Al vacancy, a He cluster favors the removal of adjacent Al atoms during bubble growth. Therefore, the growth of He cluster from the Al layer may be confined near the plane in the nucleation stage, leading to the high probability of forming platelet-like He bubbles.

The secondary defect formation energies for Ti, Al, and C are shown as a function of the number of He atoms at the primary C vacancy in Fig. 3(b). We can see that the secondary defect formation energy of the Al vacancy nearest to the primary C vacancy decreased with increasing He impurity content, changing from 2.606 eV (no He atom) to 1.033 eV (3 He atoms). An increase in the number of He atoms also decreases the defect formation energy for the nearest Ti site.

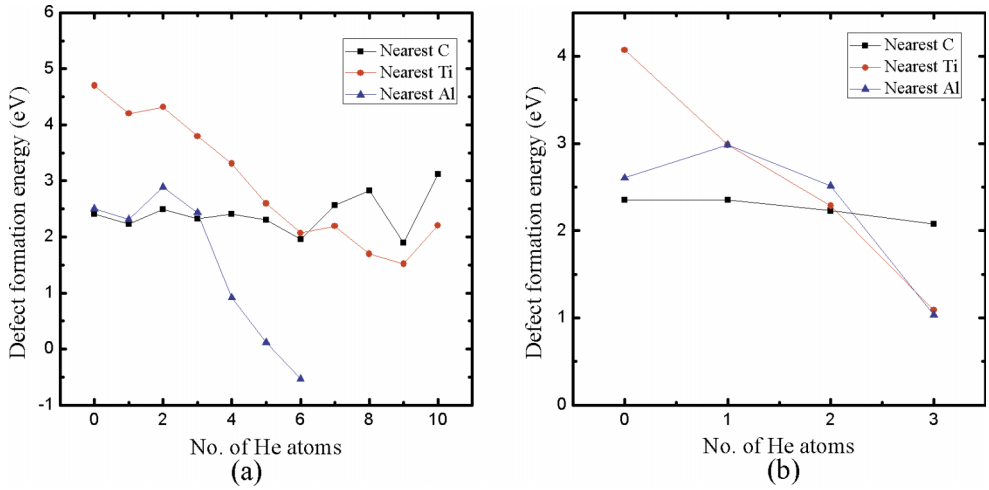

FIG. 3. The defect formation for Ti, Al, and C nearest to an Al vacancy (a) and a C vacancy (b) as a function of the number of He atoms in Ti_3AlC_2.

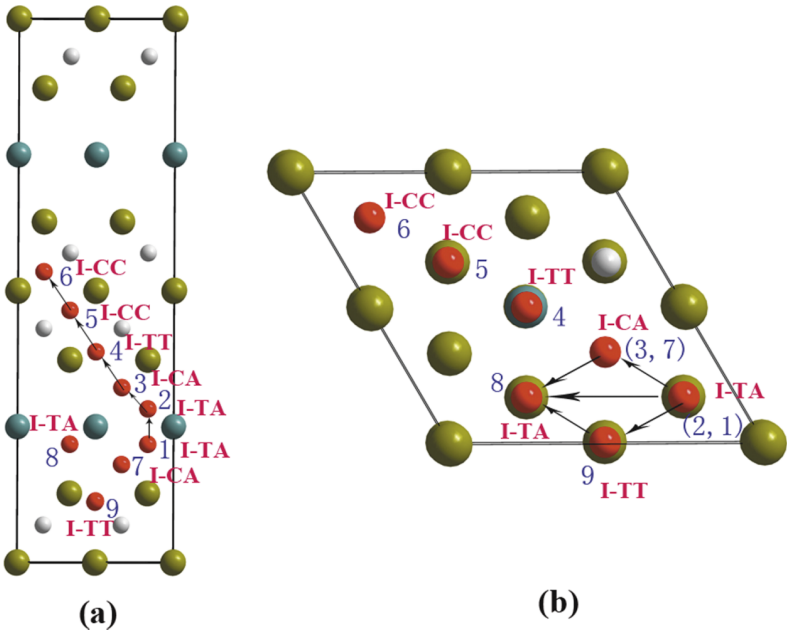

FIG. 4. Top view (a) and side view (b) of diffusion pathways for a He atom in perfect Ti_3AlC_2.

For a C vacancy without He atoms, the secondary defect formation for the Ti site is approximately 4.073 eV, whereas for a C vacancy with trapped He atoms, the defect formation energy drops to only 1.090 eV. On the other hand, the He impurity content has no obvious effect on the secondary defect formation energy of the nearest C atom site, with the energy remaining at approximately 2.2 eV. The trapping energy is also much larger than that of the Al and Ti atoms. This suggests that although C vacancies can easily form in Ti_3AlC_2, even if one vacancy is occupied by He impurities, this does not enhance the likelihood of generating secondary C vacancies nearby. Consequently, C vacancies will not cluster along a C layer but will instead nucleate to other layers (Ti or Al layers). This explains the observation that the Al layer rather than the C layer is disordered by He implantation. This also means the bubbles nucleated from C layers have a higher propensity to form a three-dimensional, i.e., spherical shape. Hence, He bubbles of different shapes are found to be nucleated from different layers of Ti_3AlC_2; according to this work, the platelet-like bubbles are more likely to be originated from Al layers and the spherical ones may be the main outcome of He clustering in C layers. When the platelets grow continuously, the adjacent platelets may link up to each other as do spherical ones.[8] As a result, string-like He bubbles can also form, as found experimentally.[11]

In the present study, to gain a deeper understanding of the dynamics of He migration on MAX phase materials, calculations for the energy barriers of different He diffusion paths in Ti_3AlC_2 are carried out. The CI-NEB method is used to find diffusion pathways and the corresponding energy barriers. Because Ti_3AlC_2 is a ceramic material characterized by a nanolaminated crystalline structure, He diffusion pathways along the *c*-axis and in the *ab* plane of the hexagonal unit cell are considered in the current study. As discussed above, I-TA is the most stable site for a He atom in perfect bulk Ti_3AlC_2. Therefore, we start our energy barrier calculations using the I-TA configuration. As illustrated in Fig. 4(a), along the *c*-axis direction, the He atom migration starts at I-TA (site 1), then proceeds to the equivalent site (site 2), then to another interstitial site I-CA (site 3), then to the I-TT (site 4), then to the next layer at the I-CC interstitial site (site 5), then to its equivalent site (site 6), and finally to the interstitial site I-TT, which is equivalent to site 4. The diffusion barriers for the 1-2, 2-3, 3-4, 4-5, and 5-6 steps of the pathway

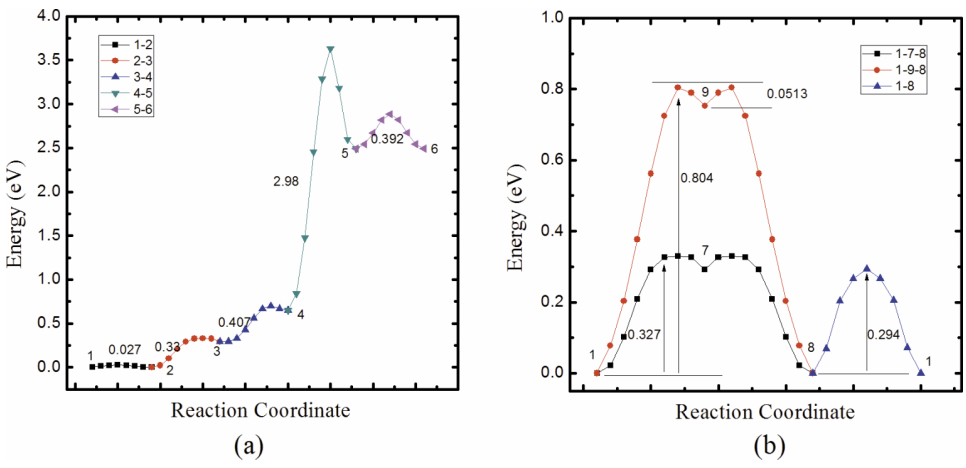

FIG. 5. Diffusion energy profile for a He atom diffusing along *c*-axis direction (a) and *a*-axis direction (b).

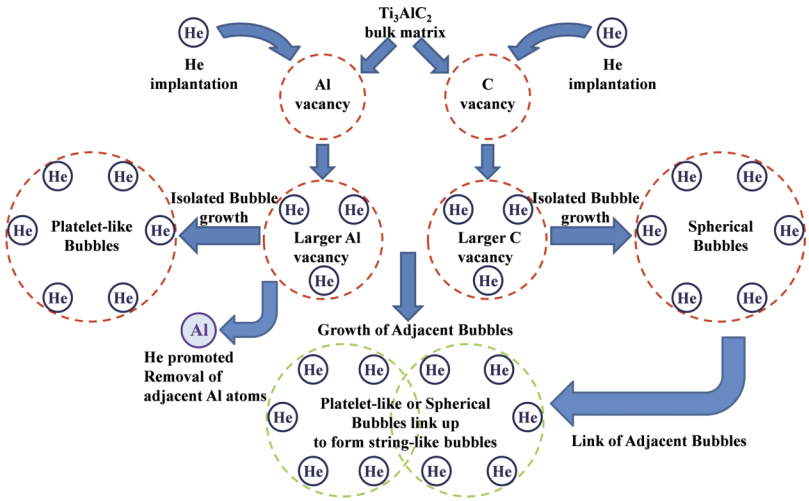

FIG. 6. Schematic diagram for the formation of bubbles in various shapes nucleated by trapped He atoms.

are 0.027 eV, 0.320 eV, 0.407 eV, 2.980 eV, and 0.392 eV, respectively, as shown in Fig. 5(a). The diffusion barrier for the 4-5 step is much higher than the other barriers and thus is the rate-determining step along the 1-2-3-4-5-6 migration path. This result may be understood as follows: when a He atom moves through a C atom layer, the transition state structure is characterized by the He atom located close to the covalent C–Ti bond. The presence of the He atom thus causes a strong distortion in the electron density of the bond; this weakens C–Ti bonding and increases the total energy, resulting in a high energy barrier. As illustrated in Fig. 4(b), in the *ab* plane, a He atom at the I-TA site (site 1) can migrate to the nearest neighbor I-TA site (site 8). There are three possible migration pathways: path 1 runs from site 1 to site 8 in a straight line (1-8 path); path 2 starts at site 1 and then passes through site 7 (I-CA), which is equivalent to site 3, ending at site 8 (1-7-8 path); and path 3 starts at site 1, passes through site 9 (I-TT), and ends at site 8 (1-9-8 path). The diffusion barrier along the 1-8 path is calculated to be 0.294 eV, lower than the value along either the 1-7-8 path (0.327 eV) or the 1-9-8 path (0.804 eV), as shown in Fig. 5(b). Therefore, the most probable path is the 1-8 path for diffusion parallel to the *ab* plane of the unit cell. It can also be readily observed that the energy barriers along the *c*-axis direction are much higher than those in the *ab* plane, so He atoms can migrate more freely in the *ab* plane, leading to faster in-plane motion and therefore faster bubble growth on the Al layer.

According to the present results, when He atoms are implanted into the MAX phase Ti_3AlC_2, they prefer to reside in the interstitial sites near the Al plane; Al vacancies in Ti_3AlC_2 exhibit strong He atom trapping; additionally, the secondary Al vacancy defect near the primary Al vacancy is the most readily produced secondary defect under the influence of He irradiation. This means that the production of planar void in Al layer to accommodate more He atoms is energetically favored with the existence of trapped He atoms. Moreover, He atoms have a lower energy barrier to move parallel to the Al plane and thus the rate growth of the He bubbles is higher along the Al plane, causing the formation of platelet-like bubbles and the platelet parallel to the Al plane. This is in excellent agreement with the observations recently reported,[11] by which it can be indicated that platelet-like bubbles are formed by He implantation and the orientation of the platelets depends only on the crystallographic orientation instead of the irradiation surface. As to the conventional spherical He bubbles, our studies indicate they are more likely to be nucleated from the C vacancies and their growth rate before the formation of a sizeable void is slower due to high energy barrier along *c*-axis. But a significant amount of spherical bubbles can still be observed in the experiments since C vacancies are determined to be dominant due to the much lower Frankel formation energy of C atoms than that of Ti and Al atoms.[23] Furthermore, string-like bubbles can form when adjacent platelet-like and spherical bubbles link together during their growth as mentioned above. Therefore, our calculations can explain the mechanism for the formation of platelet-like, spherical, and string-like He bubbles in Ti_3AlC_2, which can be schematically illustrated in Fig. 6. It should be mentioned that first principles calculations provide information on the nucleation stage of the bubble growth at the electronic structure level; larger scale modeling, such as molecular dynamics simulation or rate theory, is recommended to acquire the detail of the dynamical information on the growth process of He bubbles in Ti_3AlC_2.

It is also interesting to note that the energy barriers for He diffusion in Ti_3AlC_2, both along the *c*-axis and in the *ab* plane, are much larger than those in metals,[29–31] indicating that the rate of bubble growth in Ti_3AlC_2 is slower than that of metals. Hence, Ti_3AlC_2 possesses a higher stability against He irradiation than metals.[7,11]

IV. CONCLUSIONS

Radiation damage caused by He in the MAX phase Ti_3AlC_2 material has been investigated using first-principle methods. We find that a single He interstitial atom favors residing near the Al plane in Ti_3AlC_2. A single Al vacancy can trap ten He atoms, whereas a C vacancy can trap only three He atoms, indicating that Al vacancies are better able to trap He. The secondary defect formation energy of Al, Ti, and C vacancies nearest to the primary Al vacancy is significantly influenced by He impurity content. The secondary defect formation energy for Al vacancies is lower than that of C and Ti vacancies. The study on diffusion behavior of He in

Ti_3AlC_2 also shows that He atoms are more likely to migrate parallel to the Al plane. Therefore, He clusters trapped in Al vacancies prefer to grow into bubbles in a platelet shape orientated parallel to the Al plane. However, if the He is trapped in a C vacancy, the in-plane growth is no longer preferential and bubbles are nucleated mainly in spherical shape. As to the string-like bubbles, they are probably formed by linking of adjacent platelet-like and spherical bubbles. Thus, the mechanisms for the formation of bubbles of various shapes in Ti_3AlC_2 observed in recent experiments are elucidated according to our results. Finally, the energy barriers for He diffusion in Ti_3AlC_2 in both directions are found to be much larger than those in metals, indicating that the rate of bubble growth in Ti_3AlC_2 will be slower than that in metals, thus providing a higher stability against He irradiation. The present computational study is expected to provide new insight into the behaviors of MAX phases under extreme conditions so that MAX-based materials can be better designed.

ACKNOWLEDGMENTS

The authors acknowledge the financial support by the key technology of nuclear energy, 2014, CAS Interdisciplinary Innovation Team.

[1]P. Eklund, M. Beckers, U. Jansson, H. Hogberg, and L. Hultman, Thin Solid Films **518**(8), 1851 (2010).
[2]M. W. Barsoum, H. Yoo, I. K. Polushina, V. Y. Rud, Y. V. Rud, and T. El-Raghy, Phys. Rev. B **62**(15), 10194 (2000).
[3]X. H. Wang and Y. C. Zhou, Chem. Mater. **15**(19), 3716 (2003).
[4]D. Li, Y. Liang, X. Liu, and Y. Zhou, J. Eur. Ceram. Soc. **30**(15), 3227 (2010).
[5]K. R. Whittle, M. G. Blackford, R. D. Aughterson, S. Moricca, G. R. Lumpkin, D. P. Riley, and N. J. Zaluzec, Acta Mater. **58**(13), 4362 (2010).
[6]W. D. Wilson, C. L. Bisson, and M. I. Baskes, Phys. Rev. B **24**(10), 5616 (1981).
[7]M. K. Patel, D. J. Tallman, J. A. Valdez, J. Aguiar, O. Anderoglu, M. Tang, J. Griggs, E. Fu, Y. Wang, and M. W. Barsoum, Scr. Mater. **77**, 1 (2014).
[8]C. Wang, T. Yang, S. Kong, J. Xiao, J. Xue, Q. Wang, C. Hu, Q. Huang, and Y. Wang, J. Nucl. Mater. **440**(1-3), 606 (2013).
[9]K. F. Chen, C. H. Chen, Z. H. Zeng, F. R. Chen, and J. J. Kai, Prog. Nucl. Energy **57**(6), 46 (2012).
[10]Z. Tong and Y. Dai, J. Nucl. Mater. **385**(2), 258 (2009).
[11]P. Song, J. Sun, Z. Wang, M. Cui, T. Shen, Y. Li, L. Pang, Y. Zhu, Q. Huang, and J. Lü, Nucl. Instrum. Methods Phys. Res., Sect. B **326**, 332 (2014).
[12]Y. Zhou, Z. Sun, X. Wang, and S. Chen, J. Phys.: Condens. Matter **13**(44), 10001 (2001).
[13]A. Togo, L. Chaput, I. Tanaka, and G. Hug, Phys. Rev. B **81**(17), 174301 (2010).
[14]J. Xiao, C. Wang, T. Yang, S. Kong, J. Xue, and Y. Wang, Nucl. Instrum. Methods Phys. Res., Sect. B **304**, 27 (2013).
[15]T. Yang, C. Wang, C. A. Taylor, X. Huang, Q. Huang, F. Li, L. Shen, X. Zhou, J. Xue, and S. Yan, Acta Mater. **65**, 351 (2014).
[16]G. Kresse and J. Hafner, Phys. Rev. B **47**(1), 558 (1993).
[17]G. Kresse and J. Furthmüler, Phys. Rev. B **54**(16), 11169 (1996).
[18]P. E. Blöhl, Phys. Rev. B **50**(24), 17953 (1994).
[19]H. J. Monkhorst and J. D. Pack, Phys. Rev. B **13**(12), 5188 (1976).
[20]G. Henkelman, B. P. Uberuaga, and H. Jósson, J. Chem. Phys. **113**(22), 9901 (2000).
[21]Y. C. Zhou, X. H. Wang, Z. M. Sun, and S. Q. Chen, J. Mater. Chem. **11**(9), 2335 (2001).
[22]Y. Liu, Y. Zhang, H. Zhou, G. Lu, F. Liu, and G. Luo, Phys. Rev. B **79**(17), 172103 (2009).
[23]C. Duan, Y. Liu, H. Zhou, Y. Zhang, S. Jin, G. Lu, and G. Luo, J. Nucl. Mater. **404**(2), 109 (2010).
[24]S. C. Middleburgh, G. R. Lumpkin, and D. Riley, J. Am. Ceram. Soc. **96**(10), 3196 (2013).
[25]H. Trinkaus and B. N. Singh, J. Nucl. Mater. **323**(2), 229 (2003).
[26]H. Xu, D. Lee, J. He, S. B. Sinnott, V. Gopalan, V. Dierolf, and S. R. Phillpot, Phys. Rev. B **78**(17), 174103 (2008).
[27]H. Xu, D. Lee, S. B. Sinnott, V. Gopalan, V. Dierolf, and S. R. Phillpot, Phys. Rev. B **80**(14), 144104 (2009).
[28]H. Xu, A. Chernatynskiy, D. Lee, S. B. Sinnott, V. Gopalan, V. Dierolf, and S. R. Phillpot, Phys. Rev. B **82**(18), 184109 (2010).
[29]C. Fu and F. Willaime, Phys. Rev. B **72**(6), 64117 (2005).
[30]L. Gui, Y. Liu, W. Wang, Y. Liu, K. Arshad, Y. Zhang, G. Lu, and J. Yao, Prog. Nat. Sci.: Mater. Int. **23**(5), 459 (2013).
[31]P. Zhang, J. Zhao, and B. Wen, J. Phys.: Condens. Matter **24**(9), 95004 (2012).